



OIST

OKINAWA INSTITUTE OF SCIENCE AND TECHNOLOGY GRADUATE UNIVERSITY
沖縄科学技術大学院大学

TOB is an effector of the hippocampus-mediated acute stress response

Author	Mohieldin M. M. Youssef, Hiro Taiyo Hamada, Esther Suk King Lai, Yuji Kiyama, Mohamed El-Tabbal, Hiroshi Kiyonari, Kohei Nakano, Bernd Kuhn, Tadashi Yamamoto
journal or publication title	Translational Psychiatry
volume	12
number	1
page range	302
year	2022-07-29
Publisher	Nature Portfolio
Rights	(C) 2022 The Author(s)
Author's flag	publisher
URL	http://id.nii.ac.jp/1394/00002478/

doi: info:doi/10.1038/s41398-022-02078-7

ARTICLE OPEN



TOB is an effector of the hippocampus-mediated acute stress response

Mohieldin M. M. Youssef¹✉, Hiro Taiyo Hamada², Esther Suk King Lai³, Yuji Kiyama⁴, Mohamed El-Tabbal⁵, Hiroshi Kiyonari⁶, Kohei Nakano⁶, Bernd Kuhn⁵ and Tadashi Yamamoto¹✉

© The Author(s) 2022

Stress affects behavior and involves critical dynamic changes at multiple levels ranging from molecular pathways to neural circuits and behavior. Abnormalities at any of these levels lead to decreased stress resilience and pathological behavior. However, temporal modulation of molecular pathways underlying stress response remains poorly understood. Transducer of ErbB2.1, known as TOB, is involved in different physiological functions, including cellular stress and immediate response to stimulation. In this study, we investigated the role of TOB in psychological stress machinery at molecular, neural circuit, and behavioral levels. Interestingly, TOB protein levels increased after mice were exposed to acute stress. At the neural circuit level, functional magnetic resonance imaging (fMRI) suggested that intra-hippocampal and hippocampal-prefrontal connectivity were dysregulated in *Tob* knockout (*Tob*-KO) mice. Electrophysiological recordings in hippocampal slices showed increased postsynaptic AMPAR-mediated neurotransmission, accompanied by decreased GABA neurotransmission and subsequently altered Excitatory/Inhibitory balance after *Tob* deletion. At the behavioral level, *Tob*-KO mice show abnormal, hippocampus-dependent, contextual fear conditioning and extinction, and depression-like behaviors. On the other hand, increased anxiety observed in *Tob*-KO mice is hippocampus-independent. At the molecular level, we observed changes in factors involved in stress response like decreased stress-induced LCN2 expression and ERK phosphorylation, as well as increased MKP-1 expression. This study introduces TOB as an important modulator in the hippocampal stress signaling machinery. In summary, we reveal a molecular pathway and neural circuit mechanism by which *Tob* deletion contributes to expression of pathological stress-related behavior.

Translational Psychiatry (2022)12:302; <https://doi.org/10.1038/s41398-022-02078-7>

INTRODUCTION

On a daily basis, we encounter stressful events to which our bodies generate different responses and store memories to cope with future occurrences. The brain utilizes several mechanisms to cope with psychological stress, and defects in such mechanisms or exposure to excessive stress can increase individual vulnerability to neuropsychiatric disorders like depression and post-traumatic stress disorder (PTSD) [1]. Strikingly, it is estimated that 50% of adults have experienced a traumatic event during their lifetimes. Therefore, it is imperative that we investigate mechanisms that underlie stress responses and identify potential therapeutic targets coordinating stress resilience [2, 3].

The stress coping response is orchestrated at various intercalated layers which include brain connectivity, neuronal activity, molecular signaling, and resulting behavior [4]. Any change in stress resilience mechanisms can induce psychiatric consequences, such as increased fear, anxiety, and depression. Such behaviors are controlled by neuronal circuits governing emotional and fight-flight responses, like the hippocampus, prefrontal cortex, amygdala, and hypothalamus [5]. fMRI is currently the most

advanced, non-invasive method to map dynamic changes in brain circuits that regulate stress coping [6, 7]. The ventromedial prefrontal cortex (vmPFC) and hippocampus are regarded as critical regions for stress coping [8, 9]. The mPFC and hippocampus exhibited hemodynamic responses to acute stress [10]. In response to stress, abnormal neuronal circuit remodeling may occur, leading to altered brain connectivity in these regions. Several molecules have been implicated in these remodeling events, like lipocalin-2 (LCN2) and corticotrophin-releasing factor (CRF) [11]. The Hypothalamic-Pituitary Adrenal (HPA) axis is a hormonal signaling pathway that is moderately activated to elicit adaptation to induced stress at molecular, cellular, physiological, and behavioral levels [12]. At the molecular level, acute stress induces transcriptional and translation responses in order to cope with stress [13, 14]. This transient change in molecular signaling is believed to have neuronal protective functions [15]. Our knowledge of the hippocampal molecular stress machinery is limited; therefore, there are continuing efforts to identify genes that function in stress coping responses [16]. Interestingly, several molecules with known functions in cellular stress response have

¹Cell Signal Unit, Okinawa Institute of Science and Technology Graduate University, Okinawa, Japan. ²Neural Computation Unit, Okinawa Institute of Science and Technology Graduate University, Okinawa, Japan. ³Neural Circuit Unit, Okinawa Institute of Science and Technology Graduate University, Okinawa, Japan. ⁴Laboratory of Biochemistry and Molecular Biology, Graduate school of medical and dental sciences, Kagoshima University, Kagoshima, Japan. ⁵Optical Neuroimaging Unit, Okinawa Institute of Science and Technology Graduate University, Okinawa, Japan. ⁶Laboratory for Animal Resources and Genetic Engineering, RIKEN Center for Biosystems Dynamics Research, Kobe, Hyogo, Japan. ✉email: mohieldin.youssef@oist.jp; tadashi.yamamoto@oist.jp

Received: 23 June 2022 Revised: 14 July 2022 Accepted: 19 July 2022

Published online: 29 July 2022

also been implicated in psychological stress-coping mechanisms, e.g., EGR1 [17, 18].

Transducer of ErbB2 (TOB) has been proposed to regulate learning and memory, yet the mechanism is unknown [19, 20]. Notably, *Tob* is one of the early response genes after either neuronal depolarization in excitatory neurons or stress in humans [21, 22]. In addition, TOB protein expression is elevated in hippocampus and cerebellum after behavioral tests like fear conditioning and rotarod tests in rats, respectively [19, 20]. Moreover, decreased *Tob* gene expression has been correlated with depression [23]. Taken together, this suggests that TOB participates in neuronal molecular machinery and behavioral phenotypes. On the other hand, we previously showed that TOB exhibits a unique transient elevation after exposure to UV stress, halting apoptosis, and then eliciting an apoptotic signal after undergoing proteasome-dependent degradation [24]. In this manner, TOB allows cells to recover through DNA repair mechanisms [25]. Furthermore, overexpression of TOB in human bronchial epithelial cells leads to protection from ionizing radiation-mediated cell death, increased ERK phosphorylation, and induced expression of DNA repair proteins [26]. Stimulation using BMP-2, which induces oxidative stress, led to increased TOB protein expression [27, 28]. This suggests that TOB contributes to stress machinery, mostly protective, at both the cellular and molecular levels. However, TOB's function in psychological stress remains enigmatic.

Utilizing *Tob*-KO mice, we show that TOB has a functional role in stress coping behavior in the brain by regulating hippocampal connectivity, neuronal excitability, and temporal molecular changes induced by stress. Increased TOB protein expression in mouse brain after exposure to acute stress, accompanied by the abnormal behavioral phenotype in *Tob*-KO mice, reveals TOB as key molecular effector in the brain's stress resilience.

MATERIALS AND METHODS

Animals

Male mice with C57BL/6 J genetic background were used in this study. *Tob*-KO mouse generation and validation were described by Yoshida et al. [29]. Floxed *Tob* mice (Accession No. CDB0044E) were generated by insertion of LoxP sequences spanning exon2 of the *Tob* gene with detailed procedure described in supplementary information. Genotyping to detect insertion at the 5' end employed primers: FW 5'- TGAGAGCCCTTGGCATGG -3' REV 5'- ATACCACTTCCCAGCAGG -3' and at 3' end using: FW 5'- GGAATAATGG AAGGCAGG -3' REV 5'- CCTCTATCACCTGGCTC -3'. Mice with homozygous LoxP insertions (Floxed *Tob* mice, *Tob*^{fl/fl}) were used for experiments after backcrossing with C57BL/6 J mice for at least 5 generations. All mice were housed under controlled temperature and a 12-h light/dark cycle. The experimenters were blinded to mice genotype during experimental procedures. Exclusion criteria were determined prior to the start of experimental procedures to ensure animal welfare and were documented in animal experimental procedure protocol. Mice were allocated randomly to experimental groups following Mendelian inheritance. All animal experiments were performed following guidelines for experimental animals and approved by the Animal Care and Use Committee, Okinawa Institute and Science Technology Graduate University (OIST), Japan.

Restraint stress

Mice were restrained in 50-mL Falcon centrifuge tubes with conical bottoms (Corning, USA) for 30 min. Holes were drilled in the tubes to allow respiration, while tube caps had one hole to let their tails pass through. After restraint stress, mice were returned to their home cages for indicated times, to be sacrificed for collection of hippocampi for protein extraction.

Inescapable electric shock

Mice were exposed inescapable electric shocks as described in the training procedure for "Fear Conditioning and Extinction", and then returned to their home cages until sacrifice and collection of hippocampi at the indicated times.

Western blotting

Hippocampal tissues were lysed using ice-cold lysis buffer containing 0.3% SDS, 1.67% Triton X-100, 50 mM Tris-HCl pH7.4, 150 mM NaCl, 1 mM EDTA, 1 mM EGTA, 10% glycerol, Halt Protease inhibitor cocktail (ThermoFisher, USA), and phosphatase inhibitor cocktail PhosSTOP (Roche, Switzerland). Synaptic fractionation was done following a detailed published protocol [30]. Electrophoresis was performed using 7.5 or 12% TGX Acrylamide gels (Bio-rad, USA) following standard protocols. Proteins were transferred to PVDF membranes using Trans-Blot Turbo Transfer (Bio-Rad, USA) and blocked in TBS buffer containing 5% BSA and 0.1% Tween-20. Antibodies were diluted in Can Get Signal immunoreaction enhancer solution (Toyobo, Japan) and incubated according to the manufacturer's protocol. Antibodies used were anti-Tob mouse monoclonal antibody as described by Matsuda et al., 1996, anti-Tob rabbit polyclonal antibody (RpAb) (Sigma-Aldrich, USA), anti-ERK1/2 rabbit monoclonal antibody, anti-(p-ERK1/2) RpAb, anti-Cre RpAb (Cell Signaling, USA), anti-MKP-1 RpAb (Santa Cruz, USA), anti-LCN2 goat polyclonal antibody (R&D systems, USA). Chemiluminescent signals were generated using Immobilon (Millipore, USA) and detected using ImageQuant LAS4000 (GE healthcare, USA). For reprobing, Restore Plus stripping buffer (ThermoFisher, USA) was used. Band intensities were quantified using Image Studio Lite software (Li-Cor, USA). Automated Simple Wes system was used to quantify ERK phosphorylation levels, according to the manufacturer's instructions using the 12–230 kDa separation module and anti-rabbit detection module (ProteinSimple, USA).

Functional magnetic resonance imaging (fMRI)

Detailed head-fixation bar mounting surgery and MRI imaging procedures are described in the supplementary information.

Functional connectivity analysis

The pre-processed and denoised time series data were used for a seed-based FC analysis with CONN17. Regions of interest (ROIs) including CA1, DG, and mPFC were chosen. Seed-based functional connectivity (FC) analysis was performed to compare FC between the *Tob*-KO group and the control group. Seed-based FC analysis was composed of two steps. First, Pearson's correlation between a time series of an average seed ROI and each voxel in images was calculated, and regional clusters were formed by thresholding statistical significance (uncorrected *p*-value < 0.001) between two groups. In the second step, formed clusters were further statistically corrected with a positive false discovery rate (pFDR; *p* < 0.05).

Electrophysiological recording

Electrophysiological recordings were performed as described by Etherton et al. [31] and are detailed in the Supplementary materials and methods.

Quantitative real-time PCR

Total RNA was extracted from mouse hippocampi using Isogen II (Nippon Gene, Japan) following the manufacturer's protocol. Reverse transcription was performed using PrimeScript II 1st strand cDNA Synthesis Kit (Takara, Japan) following the manufacturer's protocol. Real-time PCR was performed using TB Green Premix Ex Taq II (Takara, Japan) and ViiA7 Real-Time PCR system (Applied Biosystems, USA). Relative mRNA expression was determined by the $\Delta\Delta$ CT method and *Gapdh* mRNA levels were used for normalization. Primers used were:

Gapdh FWD 5'- ctgaccaccaactgcttag -3' REV 5'- gtcttctgggtggcagtgat -3'; *Lcn2* FWD 5'- cccatctctgctcactgctc -3' REV 5'- tttttctggaccgattg -3'; *Crh2* FWD 5'- aagctggtgattggtggac -3' REV 5'- ggtggatgctcgtactctg -3'; *Avpr1a* FWD 5'- gctggcgggtgatttctgtg -3' REV 5'- gcaaacacctgcaagtgtc -3'; *Mc3r* FWD 5'- tccgatgctgctaacctc -3' REV 5'- ggatgtttccatcagactgacg -3'.

RNA sequencing

Intact poly(A) RNA was purified from 1 μ g of total RNA using an NEBNext® Poly(A) mRNA Magnetic Isolation Module (New England Biolabs, USA) and following the manufacturer's protocol. Library preparation was performed using NEBNext® Ultra II Directional RNA Library Prep Kits for Illumina (New England Biolabs, USA), according to the manufacturer's protocol with 8 PCR cycles. Library sizes were checked using microfluidic-based electrophoresis LabChip GX Touch (Perkin Elmer, USA) and concentrations were checked using Qubit 1X dsDNA HS (ThermoFisher, USA) and then pooled after concentration adjustment. 150-bp paired-end RNA sequencing was performed using a NovaSeq 6000 SP flow cell (Illumina, USA).

Analysis was done using fastq files containing paired-end sequencing reads and analyzed using nf-core/rnaseq pipeline v2.0 [32], which were mapped to the GRCh38 genome database using STAR aligner (v2.6.1d) [33]. Mapped genes were then further analyzed using OmicsBox software (v1.4.11) for counting using HTSeq (v0.9.0) [34] and differential gene expression analysis using the package EdgeR (v3.11) [35]. Reads were normalized using the Trimmed Mean of M-values (TMM) normalization method and a cut-off of at least 0.2 counts per million (CPM) in two samples was selected. Differentially expressed genes (DEGs) were statistically tested using EdgeR's exact test, and genes with $FDR \leq 0.05$, $p\text{-value} \leq 0.05$ and fold change (FC) ≥ 2 or ≤ -2 were used for further analysis. Pathway analysis was performed for genes 2-fold up- or down-regulated with $p\text{-value} < 0.05$ using Ingenuity Pathway Analysis (IPA) software (Qiagen, USA).

Raw and pre-processed transcriptomic data files described in the current study are publicly available in NCBI GEO under accession number GSE186101.

Behavior

Behavioral analyses were performed using male mice 8–12 weeks old. All experiments were performed by experimenters blinded to genotype during testing. All software for analysis was from O'Hara & Co Ltd., which has been modified in the public domain (National Institutes of Health (NIH) Image J program).

Fear Conditioning and extinction

Fear conditioning and extinction were performed as described previously by Pibiri et al., (2008) [36] with minor modifications. Briefly, on training day, mice were placed in a conditioning chamber (CL-3002L, O'Hara & Co Ltd., Japan) for 2 min to habituate, and then presented with a conditioning stimulus (CS) of a 65-dB tone for 30 s, co-terminated with an unconditioned stimulus (US) of 0.5 mA, a 2-s foot shock. The tone and foot shock were repeated 3 times at 2-min intervals. Mice were returned to their home cages 30 s after the last shock. During the contextual fear test (Day 1), mice were placed in the chamber for 5 min without any tone or shock presentation. During cued fear conditioning, mice were placed in a novel chamber for 6 min and allowed to explore then presented with a tone for 3 min. Then contextual fear extinction was tested by placing the mice for 5 min in the same context used for CS-US conditioning for 5 consecutive days (Days 2–6) with no tone or shock presentation. Freezing was recorded during each test and analyzed using Image FZC 2.22 sr2 software (O'Hara & Co Ltd., Japan).

Forced swim test

The forced swim test was performed as described by Inoue et al. [37]. Briefly, mice were placed in water-filled cylinder for 10 min. Immobility was recorded and analyzed starting from the third minute using Time software (O'Hara & Co Ltd., Japan).

Elevated-plus maze test

The maze consisted of two open and two closed arms with dimensions (25 cm length \times 5 cm width), which were elevated 50 cm above the floor. Mice were placed in the center region facing one of the open arms and allowed to move freely for 10 min. Time spent in open arms was recorded and analyzed using Time EPC software (O'Hara & Co Ltd., Japan).

Open field test

Mice were placed in the center of an open field arena with dimensions (50 \times 50 \times 33.3 cm; width, depth and height) and 100 lux illumination intensity and allowed to freely move for 15 min. Movement traces, speed, distance traveled, and time spent in the center of the open field were recorded and analyzed using Time OFCR software (O'Hara & Co Ltd., Japan).

Tail suspension test

Mice were suspended by their tails for 6 min. Immobility duration was recorded and analyzed using Time software (O'Hara & Co Ltd., Japan).

Adeno-associated virus (AAV) production

AAV serotype 9 expressing mouse *Tob* under control of the human synapsin promoter (hSyn) was generated as described by Kudo et al.,

(2020) [38]. Briefly, pAAV2-hSyn-mTob was generated from pAAV2-hSyn-EGFP (Addgene, USA) by replacing the EGFP sequence with mouse *Tob* coding sequence. AAV-293 cells (Agilent, USA) were transfected with AAV-rep2/cap9 expression plasmids, adenovirus helper plasmids, and AAV-vector plasmids to generate AAV9-hSyn-mTob.

Stereotaxic surgery for viral injection

Tob^{fl/fl} mice were bilaterally injected with Cre-expressing adeno-associated virus AAV1.hSyn.Cre.WPRE.hGH (105553-AAV1, Addgene) to generate hippocampus-specific KO mice. *Tob*-WT and KO mice were injected with AAV to express mouse TOB AAV9.hSyn.mTob.WPRE.hGH for rescue experiments. Stereotaxic surgical procedures were performed as described by Augustinaite and Kuhn [39]. Briefly, mice were anesthetized using an intraperitoneal injection of a mixture of Medetomidine (0.3 μ g/g), Midazolam (5 μ g/g) and butorphanol (5 μ g/g). Additionally, a non-steroidal anti-inflammatory, Carprofen (7.5 μ g/g), was injected by the end of the surgery. Mice were fixed on a stereotaxic frame and head hair was shaved. A 2% lidocaine solution was applied to the shaved skin and left for 2 min. Iodine was applied gently over the skin as an antiseptic. A midline incision was made, and skin was retracted, and the skull was exposed. After drying the surface, the bregma was detected. A micromanipulator was used to slowly move the injection needle to the target injection site. A dental drill was used to drill a small hole, until the surface of the brain appeared. A needle with viral solutions of around 300 nL was slowly advanced into the hole until it touched the brain surface, and slowly lowered to the target coordinates. Injection was done over 2 min and thereafter, the needle was left in place for 5 min before slowly retracting it. Coordinates used for the CA1 region of the hippocampus were tested and optimized as 1.6 mm posterior, 1.5 mm medio-lateral and 1.6 mm ventral to the bregma.

Immunohistochemistry

Immunohistochemical staining was performed as described by Matsuura et al. [40]. Antibodies used were Anti-Cre RpAb (Cell Signaling, USA) and Alexa Flour 488 Goat Anti-rabbit IgG (Invitrogen, USA).

Statistical analysis

All data are presented as means \pm SEMs. Each replicate corresponds to a biological replicate. There was no significant difference between variances for groups undergoing statistical analyses. Data used for statistical analyses passed the normality test. T-tests, Mann-Whitney U test, one-way ANOVA, and two-way ANOVA were used as described in figure legends. Multiple comparisons following ANOVA were corrected using Bonferroni or Dunnett's *post-hoc* tests. GraphPad prism 9 was used to perform all statistical analyses.

Sample size was calculated using OpenEpi v3 software. We calculated the animal subject sample size by comparing the mean differences and standard deviation values for two genotypes from two different behavioral experiments data at 95% confidence interval, 80% power and ratio between groups is 1. The optimum sample size results were 3 and 6 animals for each genotype group.

RESULTS

TOB protein increases in response to stress

TOB's function as an anti-proliferative protein is well known, but the potential role it plays in regulating brain function is not well understood [19–21, 23, 41, 42]. With this objective, we analyzed levels of TOB protein in mouse brain. We show that TOB is ubiquitously expressed across various regions of mouse brain (Fig. 1A). Effector proteins controlling neuronal functions usually show synaptic expression patterns [43]. Likewise, TOB protein is localized in the neuronal synaptic fraction, including synaptoneuroosomes and post-synapses (Fig. 1B). TOB responds to cellular stress, neuronal activation, and glucocorticoid stimulation [21, 22, 24]. Therefore, we examined whether TOB protein levels change in response to acute psychological stress. Restraint stress and inescapable electric shock are widely used models of acute psychological stress [44, 45]. The hippocampus is associated with responses to acute stress [46] and in the hippocampus, TOB

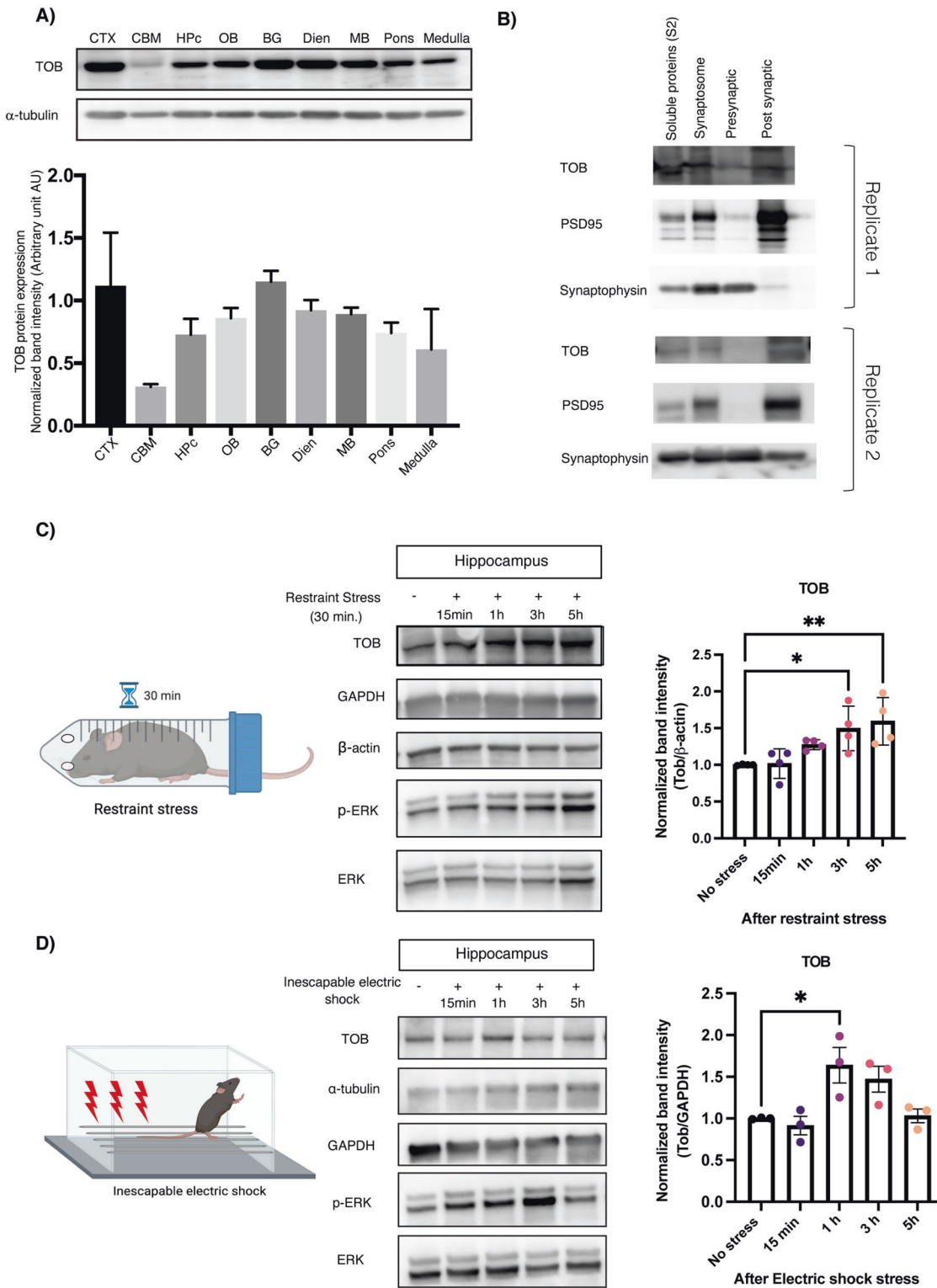
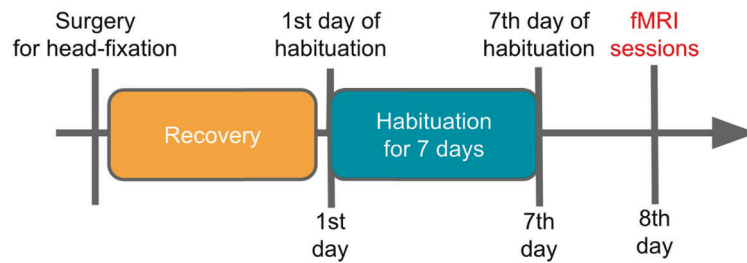
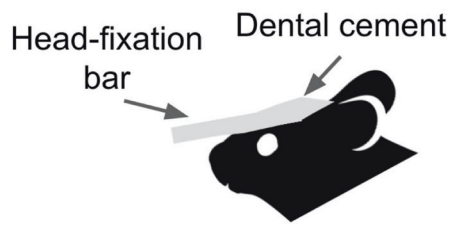


Fig. 1 TOB protein expression levels increase in response to stress. **A** Expression patterns of TOB in lysates of different mouse brain regions ($n = 3$). **B** Immunoblotting of TOB, synaptophysin, and PSD-95 in hippocampal fractionated lysates: soluble fraction S2, synaptoneurosome, pre-synaptic, and post-synaptic fractions. **C** Western blotting of TOB expression levels in hippocampal lysates without stress and after 30 min of restraint stress at different times: 15 min, 1 h, 3 h, 5 h after stress exposure ($n = 4$). **D** Western blotting of TOB expression levels in hippocampal lysates without stress and after inescapable electric shock for different durations: 15 min, 1 h, 3 h, 5 h post-exposure to stress ($n = 3$). One-way analysis of variance (ANOVA) followed by Dunnett’s post-hoc correction for multiple comparisons: statistical significance $*p < 0.05$ $**p < 0.01$ when compared to control (No stress). Data are presented as means \pm SEMs.

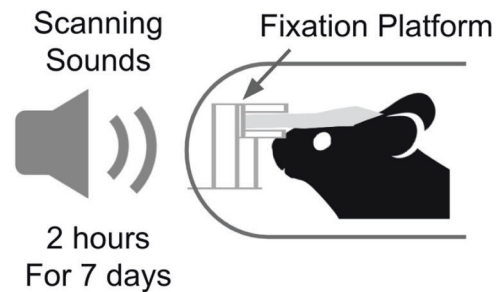
A) Experimental Schedule



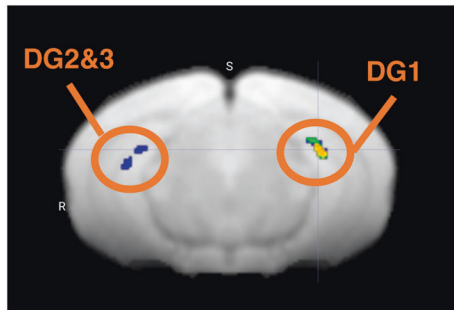
B) Surgery



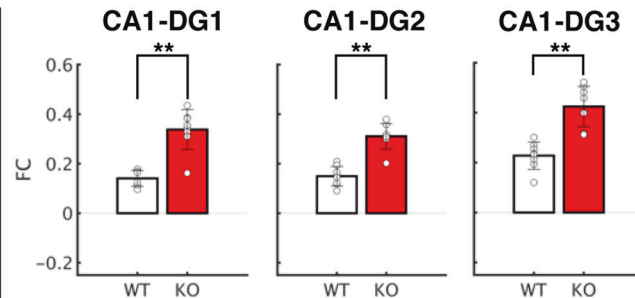
C) Habituation Training



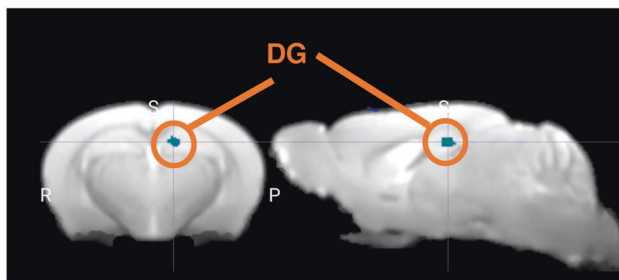
D)



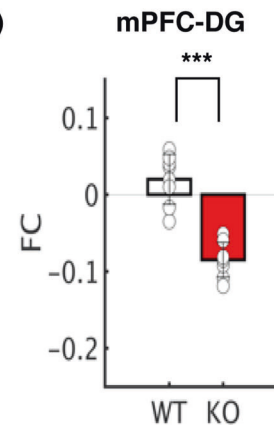
E)



F)



G)



protein increased by 49.5% and 59.3% at 3 and 5 h ($F_{4,15} = 6.050$, $p = 0.0042$; No stress vs 3 h $p = 0.0205$ and No stress vs 5 h $p = 0.0058$) post-exposure to 30 min of restraint stress, respectively, compared to non-stressed mice (Fig. 1C). Additionally, hippocampal TOB increased by 63.8% ($F_{4,10} = 5.849$, $p = 0.0108$;

No stress vs 1 h $p = 0.0221$) 1 h after mice were introduced to inescapable electric shock stress (Fig. 1D). ERK phosphorylation levels also increased after acute stress, concurrently with TOB expression. Thus, TOB is expressed in the mouse brain and its expression is increased following acute stress.

Fig. 2 Deletion of *Tob* alters brain functional connectivity. **A** Experimental Schedule. After surgery to introduce a head-fixation bar on the skull, mice were allowed to recovery. After recovery periods, mice underwent habituation training 2 h for 7 days prior to fMRI sessions. **B** Surgery. A plastic head-fixation bar was mounted on the skull with dental cement. **C** Habituation Training. In order to reduce scanning stress, mice were fixated with a fixation platform, and their bodies were constrained in a plastic tube. They were exposed to scanning sounds for 2 h for 7 days in order to reduce stress responses. **D** Statistical functional map with the seed region, CA1. Average BOLD signals were extracted from bilateral CA1. Seed-based functional connectivity was performed, and a statistical map was visualized ($p < 0.05$ after cluster correction; Fig. S1). **E** Functional connectivity with the bilateral CA1 seed. Seed-based FC analysis revealed statistically significant FC in CA1-DG1-3 in the *Tob* KO group with Mann-Whitney U test (** $p < 0.01$ with Bonferroni Correction). **F** Statistical functional map with the seed region, mPFC. Average BOLD signals were extracted from the mPFC. Seed-based functional connectivity was performed, and a statistical map was visualized ($p < 0.05$ after cluster correction; Fig. S1). **G** Functional connectivity with the mPFC seed. Seed-based FC analysis revealed statistically significant FC in mPFC-DG in the *Tob* KO group (** $p < 0.001$ with Bonferroni Correction).

Deletion of *Tob* alters the brain's functional connectivity

Next, we sought to investigate the functional influence of *Tob* deletion on brain activity with resting-state functional magnetic resonance imaging (rs-fMRI) in the awake state with habituation to a small rodent MRI scanner. Awake resting-state fMRI for small animals allows us to observe brain-wide synchronization of hemodynamic signals across multiple brain regions. Prior to awake rs-fMRI sessions, *Tob*-KO and WT groups underwent habituation training for 7 days in a mock MRI environment with MRI scanning sounds (Fig. 2A–C). In order to check functional association with hippocampal CA1 and mPFC, we performed seed-based functional connectivity (FC) analysis and contrasted *Tob*-KO and WT groups. The seed-based FC analysis with bilateral CA1 revealed the statistical significance of FC with Dentate Gyrus (DG; $p < 0.05$ with FDR correction, Fig. 2D) and the primary somatosensory area (PSSA; $p < 0.05$ with FDR correction; Fig. S1). The previous analysis of CA1 revealed positively higher FC with DG and negatively higher FC with PSSA ($p < 0.01$ by Mann-Whitney U test; Fig. 2E). Furthermore, the seed-based FC analysis with mPFC revealed the statistical significance with DG ($p < 0.05$ with FDR correction; Fig. 2F) and SMA (SMA; $p < 0.05$ with FDR correction; Fig. S1). The previous analysis of mPFC also showed negatively higher FC with DG and SMA ($p < 0.01$ by Mann-Whitney U test; Fig. 2G). Our results imply that *Tob* KO may influence functional associations within hippocampal complex (HC) and between HC and mPFC.

Altered excitatory/inhibitory balance in *Tob*-KO hippocampal slices

To test whether *Tob* deletion alters synaptic function, we performed whole-cell patch clamp recordings in hippocampal CA1 pyramidal neurons in acute brain slices. We first investigated excitatory synaptic transmission in hippocampal CA1 pyramidal neurons. We found that *Tob* deletion significantly increased the amplitude (Fig. 3B), but not the frequency (Fig. 3C) of spontaneous miniature excitatory postsynaptic currents (mEPSC) when compared to WT mice. This selective change in mEPSC amplitude suggests that *Tob* deletion may enhance the number of postsynaptic receptors and/or the size of released presynaptic vesicles.

We further explored whether AMPA and NMDA receptors, the two major glutamate receptor classes mediating fast excitatory synaptic transmission, contribute to the dysregulation after *Tob* deletion (Fig. 3A–C). We characterized AMPA receptor-mediated synaptic transmission at CA3-CA1 synapses in the hippocampus by assessing the input (stimulation intensity)-output (EPSC amplitude) efficiency and voltage dependence of synaptic AMPA-mediated synaptic responses in the presence of the NMDA receptor antagonist, D-APV. Slopes of the linear fit for individual AMPA-mediated input-output experiments were significantly different in KO mice compared to those of WT ($p = 0.0039$) (Fig. 3D). No apparent difference between genotypes was found in the current-voltage (I - V) curve (Fig. 3E). The rectification index of AMPA receptor-mediated responses from *Tob*-KO was also comparable to that of WT (WT: 0.861 ± 0.08 ; KO: 0.783 ± 0.07 ; $p = 0.568$ with the Mann-Whitney U test). Moreover, AMPA

receptor-mediated, paired-pulse facilitation was slightly increased in KO synapses (Fig. 3F), most pronouncedly at 10-ms inter-pulse intervals ($p = 0.032$). This suggested that *Tob* deletion resulted in an increase in the number of mature postsynaptic AMPA receptors without changing the AMPA receptor subunit composition.

We next investigated NMDA receptor-mediated synaptic transmission at CA3-CA1 synapses in the hippocampus. We measured the input-output relationship and I - V curve of synaptic NMDA receptor-mediated synaptic responses in the presence of the AMPA receptor antagonist, NBQX. We found no apparent differences between genotypes (Fig. S2A, B). The rectification index of NMDA receptor-mediated responses from *Tob*-KO was also similar to that of wild-type (WT: 2.959 ± 0.444 ; KO: 2.032 ± 0.136 ; $p = 0.135$ with the Mann-Whitney U test).

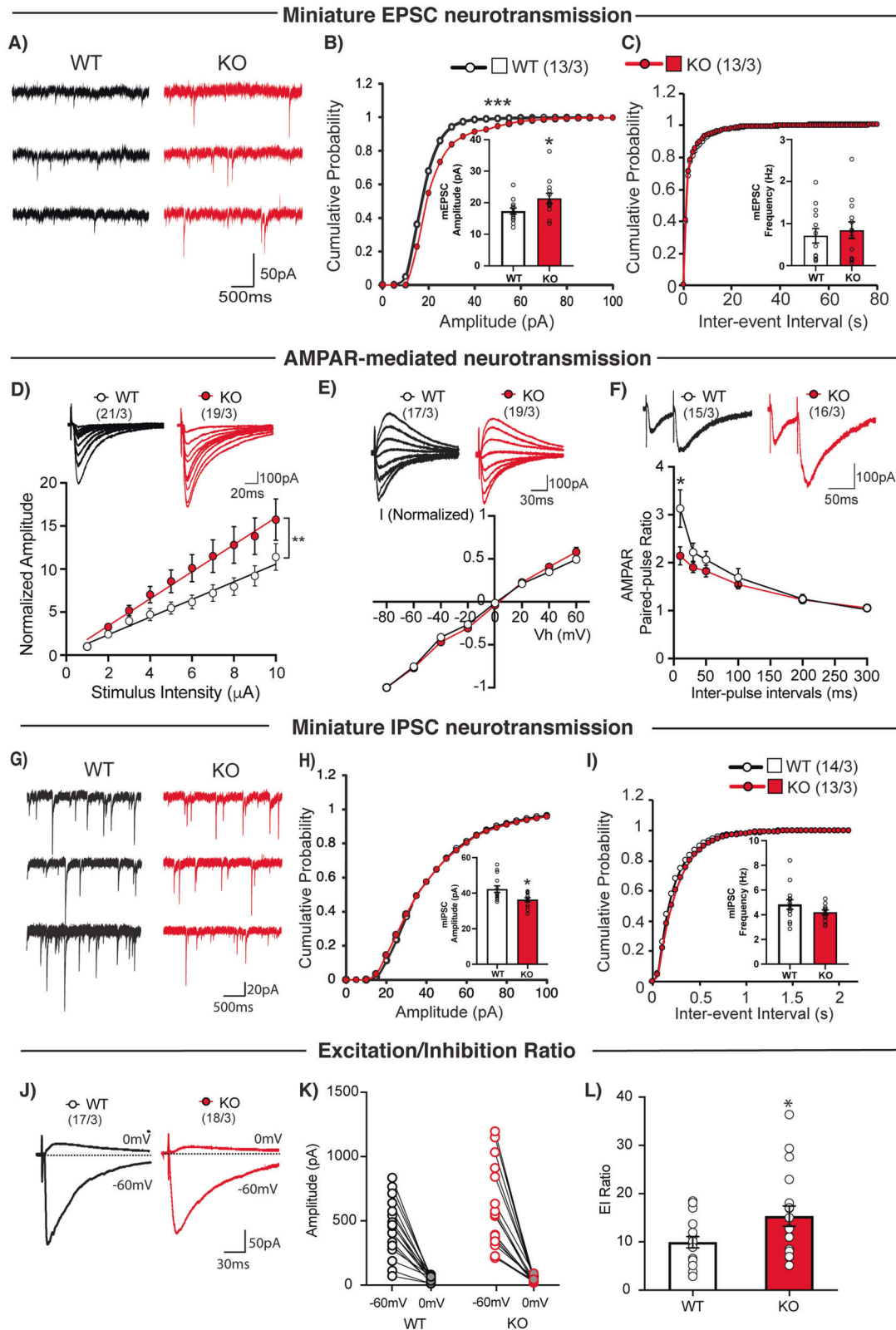
We further examined inhibitory synaptic functions in hippocampal CA1 pyramidal neurons. The amplitude (Fig. 3H), but not the frequency (Fig. 3I) of miniature inhibitory postsynaptic currents (mIPSCs) were reduced in *Tob*-KO mice, compared to that of wild-type mice (Fig. 3G–I). These results indicate that *Tob* deletion affects both excitatory and inhibitory synaptic transmission.

Next, we directly estimated the ratio of excitation to inhibition in hippocampal pyramidal neurons. We first recorded AMPA receptor-mediated EPSCs at a holding potential of -60 mV, equivalent to the Cl^- equilibrium potential. Then we recorded GABA_A receptor-mediated IPSCs at a holding potential of 0 mV, which is the reverse potential of AMPA and NMDA receptors. We then calculated the ratio of EPSC amplitude to that of IPSC amplitude (E/I ratio) and found that the E/I ratio was markedly increased in *Tob*-KO mice (Fig. 3J–L).

Tob-KO mice show abnormal stress-related behavior

Contextual fear conditioning includes exposing mice to aversive acute stress caused by inescapable electric shocks. Then brain regions respond by associating the context to such a stimulus. Fearful mice freeze when exposed to the same context in which conditioning occurred. On the other hand, contextual fear extinction is the subsidence of fear response due to repetitive exposure to the same context without shock presentation [47]. After fear conditioning, *Tob*-KO mice exhibited increased contextual fear freezing ($F_{3,30} = 10.77$, $p < 0.0001$ for genotype effect; $F_{15,150} = 2.727$, $p = 0.0010$ for time \times genotype effect; WT vs KO at Day 1 $p < 0.0001$, Day 2 $p < 0.0001$, Day 3 $p = 0.0003$, Day 4 $p = 0.0342$) (Fig. 4A). Overexpression of *Tob* in the hippocampus rescued the abnormal fear phenotype as *Tob*-KO (AAV_mTob) did not exhibit significant fear compared to *Tob*-WT (AAV_mTob) any time after conditioning. Additionally, KO mice rescued through overexpression of AAV_mTob, showed significantly less freezing when compared to KO (KO(AAV_mTob) vs KO at Day 1 $p < 0.0001$, Day 2 $p < 0.0001$, Day 3 $p = 0.0058$) (Figs. 4A, S3 A–D). *Tob* deletion in the hippocampus causes an increased fear response to an aversive context and decreased extinction, which was reversed by re-expression of *Tob*.

The forced swim test, in which immobility is associated with increased despair, is widely used to test depression-like



behavior, but it is also an efficient test of the ability to cope with stress [48]. *Tob*-KO mice showed increased immobility in the forced swim test ($F_{3,28} = 13.50$, $p < 0.0001$; WT vs KO $p = 0.0003$). Re-expression of TOB in the hippocampus of *Tob*-KO mice reduced immobility (KO(AAV_mTob) vs KO $p = 0.0008$;

WT(AAV_mTob) vs KO(AAV_mTob) $p > 0.9999$) (Fig. 4B). Similarly, we observed increased immobility by *Tob*-KO mice in the tail suspension test, which was rescued by TOB overexpression in the hippocampus (Fig. S3E). This shows that TOB in the hippocampus is important for coping with stress.

Fig. 3 **Altered excitatory/inhibitory balance in *Tob*-KO hippocampal slices.** **A** Representative traces of mEPSCs recorded from hippocampal pyramidal neurons of wild-type (WT, left traces) and *Tob* knockout (KO, right traces) at Vh of -70 mV in the presence of 1 μ M tetrodotoxin and 100 μ M PTX. Scale bars, 50 pA and 500 ms. **B** Cumulative distribution plots and summary bar graphs for mEPSC amplitude (inset shows the average mEPSC amplitude) in CA1 hippocampal pyramidal neurons of wild-type (white column) and *Tob*-KO (gray column) mice. *** $p < 0.0001$ by Kolmogorov-Smirnov test in the cumulative distribution plot and * $p = 0.0453$ by unpaired Student's *t* test in the bar graph. **C** Cumulative distribution plots and summary bar graphs for the mEPSC inter-event interval (inset shows the average of mEPSC frequency) in CA1 hippocampal pyramidal neurons of wild-type (white column) and *Tob*-KO (gray column) mice. $p = 0.4611$ by Kolmogorov-Smirnov test in the cumulative distribution plot and $p = 0.6164$ by unpaired Student's *t* test in the bar graph. **D** Sample traces (upper panel) and summary plots for the input-output relationship of AMPA receptor-mediated responses recorded from wild-type (open circles) and *Tob*-KO (gray circles) mice. Scale bars, 100 pA and 20 ms. ** $p = 0.0039$ by Mann-Whitney U test. **E** Sample traces (upper panel) and summary plots for the *I*-*V* curve of AMPA receptor-mediated responses recorded from wild-type (open circles) and *Tob*-KO (gray circles) mice. Scale bars, 100 pA and 30 ms. **F** Sample traces with 50-ms inter-pulse interval (upper panel) and summary plots for paired-pulse ratio of AMPA receptor-mediated responses at 10, 30, 50, 100, 200, and 300 ms inter-pulse intervals recorded from wild-type (open circles) and *Tob*-KO (gray circles) mice. Scale bars, 100 pA and 50 ms. * $p = 0.0139$ by Mann-Whitney U test; *** $p < 0.0011$ by Two-way ANOVA with Sidak's multiple comparisons test. **G** Representative traces of mIPSCs recorded from hippocampal pyramidal neurons of wild-type (WT, left traces) and *Tob*-KO (KO, right traces) at Vh of -70 mV in the presence of 1 μ M tetrodotoxin and 100 μ M PTX. Scale bars, 20 pA and 500 ms. **H** Cumulative distribution plots and summary bar graphs for mIPSC amplitude (inset shows the average of mIPSC amplitude) in CA1 hippocampal pyramidal neurons of wild-type (white column) and *Tob*-KO (gray column) mice. * $p = 0.0120$ by unpaired Student's *t* test in the bar graph. **I** Cumulative distribution plots and summary bar graphs for the mIPSC inter-event interval (inset shows the average of mIPSC frequency) in CA1 hippocampal pyramidal neurons of wild-type (white column) and *Tob*-KO (gray column) mice. $p = 0.9311$ by Kolmogorov-Smirnov test in the cumulative distribution plot and $p = 0.1633$ by unpaired Student's *t* test in the bar graph. **J** Representative traces of evoked EPSCs at Vh = -60 mV and evoked IPSCs at Vh = 0 mV in wild-type (left) and *Tob*-KO (right) mice. Scale bars, 50 pA and 30 ms. **K** Amplitudes of evoked EPSCs at Vh of -60 mV and evoked IPSCs at Vh of 0 mV at each of individual recorded WT and *Tob*-KO hippocampal pyramidal neurons. **L** Average excitation/inhibition ratio from WT (open column) and *Tob*-KO (gray column). * $p = 0.0343$ by unpaired Student's *t* test. Data are expressed as means \pm SEMs. Total numbers of cells recorded/total numbers of mice used are indicated in parentheses.

Since anxiety is usually observed in models showing abnormal stress coping mechanisms, we next analyzed anxiety in our mouse model. *Tob*-KO mice spent less time in the open arm of the elevated-plus maze, an indication of increased anxiety ($F_{3,30} = 3.948$, $p = 0.0174$; WT vs KO $p = 0.0283$) (Fig. 4C). Unlike in fear conditioning, TOB re-expression in hippocampus did not decrease anxiety in KO mice, as time spent in the open arm was not significantly different.

In the open-field test, *Tob*-KO mice spent less time in the center region than WT mice ($F_{3,37} = 4.263$, $p = 0.0111$; WT vs KO $p = 0.0309$; WT(AAV_mTob) vs KO(AAV_mTob) $p = 0.3621$) (Fig. 4D, S3 F-H). Although the time spent in center region was still low after overexpression of AAV_mTob in the hippocampi of KO mice, there was no significant difference between WT(AAV_mTob) and KO(AAV_mTob). Therefore, we believe that the increased anxiety in *Tob* KO mice is not hippocampus-dependent.

In order to identify specific brain areas associated with *Tob* behavioral deficiencies, we generated hippocampus-specific *Tob*-KO mice (hsTobKO) using the Cre-loxP system. First, loxP sequences flanking exon2 were inserted in the *Tob* gene (*Tob*^{fl/fl}) (Fig. S4A). Adeno-associated virus expressing Cre recombinase under the human synapsin 1 (*hSyn*) promoter (AAV_hSyn_Cre) was injected into the dorsal hippocampus of *Tob*^{fl/fl} mice to delete *Tob* specifically in this region in adult mice (Figs. 4E, S4B, C). We then analyzed behavior of hsTobKO mice. Freezing in the same context, where mice had undergone fear conditioning, and subsequent extinction trials were increased after TOB deletion in hippocampus ($F_{1,14} = 26.11$, $p = 0.0002$ for genotype effect; $F_{5,70} = 4.701$, $p = 0.0009$ for time \times genotype effect; AAV_hSyn_Cre vs *Tob*^{fl/fl} at Day 1 $p < 0.0001$, Day 2 $p < 0.0001$, Day 3 $p = 0.0148$, Day 4 $p = 0.1301$) (Fig. 4F). Additionally, hsTobKO did not show abnormal cued fear (Fig. S4D, E). Depression-like behavior was observed in hsTobKO mice in that immobility time was higher during the forced swim test (t-test $p = 0.0193$; Fig. 4G), and tail suspension test (Fig. S4F). On the other hand, anxiety levels were normal, and time spent in the open arm did not differ in hsTobKO and *Tob*^{fl/fl} mice (t-test $p = 0.3329$) (Fig. 4H). Also, no abnormal anxiety was observed in hsTobKO mice, as there was no change in time spent in the center of the open field test (t-test $p = 0.0972$) was observed (Fig. 4I, S4G-H). Negative control was utilized to exclude any possible effects associated with the surgical procedure and/or viral virulence, this was done through

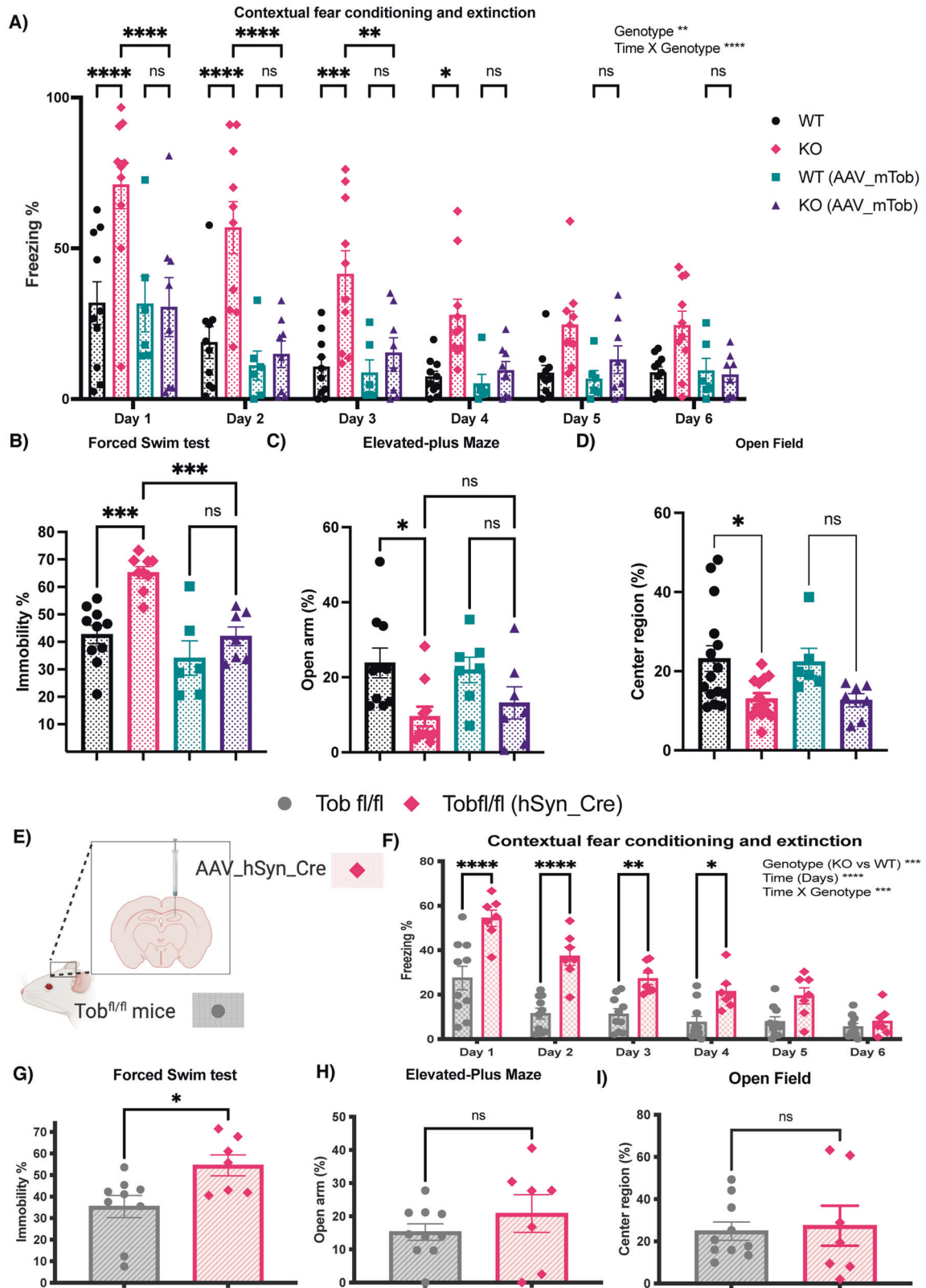
injecting *Tob*^{fl/fl} with AAV-expressing GFP (hSyn_GFP). There was no significant difference when comparing *Tob*^{fl/fl} (hSyn_GFP) to *Tob*^{fl/fl} (Fig. S5A-D). These results show that TOB in the hippocampus is important for normal fear and depression behaviors.

Abnormal transient transcriptional profile in hippocampus of *Tob* KO mice and suppressed stress-induced LCN2 expression induced after fear conditioning

Stress stimulates neuronal activation, which in return induces changes in the underlying molecular signaling pathways. Abnormal responses at the molecular level would lead to aberrant stress coping behavior. Since *Tob*-KO mice showed increased contextual fear and abnormal extinction, we analyzed hippocampal transcriptomic changes after fear conditioning. To analyze rapid changes resulting from aversive stimuli in fear conditioning, we performed RNA sequencing on hippocampal RNA from mice culled at 15 min, 1 h, and 3 h post-conditioning, in addition to naive mice. When compared to WT mice, differentially expressed genes in *Tob*-KO mice were 3,3,2 upregulated and 2,1,3 down-regulated genes for naive mice, and 1 h and 3 h post-training, respectively (Fig. 5A). Strikingly, the greatest differential transcriptome changes in *Tob*-KO occurred 15 min after conditioning, in that 26 genes were upregulated and 11 genes were down-regulated (EdgeR WT vs KO 15 min after fear conditioning, $p < 0.05$, FDR < 0.05). Therefore, TOB deletion altered the rapid change in the hippocampal transcriptome after fear conditioning.

To understand the possible molecular pathway governing this transcriptomic change, we performed pathway analysis. Pathway analysis for differentially expressed genes 15 min after fear conditioning suggested upstream activation of hormone concentration, estrogen receptor 1 (*Esr1*) and dexamethasone-induced pathways with genes for receptors controlling the HPA axis and corticoids like *Mc3r*, *Crhr2*, *Avpr1a* and neuronal inflammation genes like *Lcn2* (Figs. 5B and S6A-E).

Lipocalin-2 (*Lcn2*) was one of the transcripts downregulated in hippocampi of *Tob*-KO mice. To confirm this, we performed qRT-PCR, which showed lower mRNA levels in hippocampi of *Tob*-KO mice for naive and 15 min post-fear conditioning ($F_{1,16} = 27.4$, $p < 0.0001$ for Genotype effect; $F_{3,16} = 14.22$, $p < 0.0001$ for Genotype \times time effect; WT vs KO naive $p = 0.0363$, 15 min $p < 0.0001$) (Fig. 5C). Lower *Lcn2* mRNA levels coincided with lower



protein levels, in which fear conditioning-induced LCN2 protein expression after 15 min was suppressed in *Tob*-KO mice ($F_{1,4} = 11.67$, $p = 0.0269$ for Genotype effect; $F_{3,12} = 5.199$, $p = 0.0157$ for Time x Genotype; WT vs KO 15 min $p = 0.0007$) (Fig. 5D, E). These results show that TOB contributes to activation of stress-induced LCN2 transcription and subsequent translation.

Additionally, fear-induced ERK phosphorylation was inhibited in hippocampi of KO mice after fear conditioning ($F_{1,24} = 7.395$, $p = 0.0120$ for Genotype effect) (Figs. 5F, G, S7G). On the other hand, MKP-1 protein levels were elevated in KO mice ($F_{1,3} = 12.25$, $p = 0.0395$ for Genotype effect; $F_{3,9} = 5.358$, $p = 0.0216$ for Time x Genotype; WT vs KO 1 h $p = 0.0124$, 3 h $p = 0.0029$).

Fig. 4 **Tob-KO mice show hippocampal-mediated abnormal stress-related behavior.** Behavioral analyses in *Tob*-WT and KO mice and after overexpression of mouse TOB using AAV (hSyn-mTob) **A–D**. **A** Contextual fear conditioning and extinction expressed as percentage of time spent freezing. Two-way ANOVA followed by Bonferoni's *post-hoc* test for multiple comparisons. **B** The forced swim test presented as a percentage of immobile time. One-way ANOVA followed by Bonferoni's *post-hoc* test for multiple comparisons. **C** Elevated-plus maze showing the percentage of time spent in open arm. One-way ANOVA followed by Bonferoni's *post-hoc* test for multiple comparisons. **D** Open field test showing the percentage of time spent in center region. One-way ANOVA followed by Bonferoni's *post-hoc* test for multiple comparisons. Behavioral analyses in hippocampal-specific *Tob*-KO mice (E–I). **E** Schematic diagram showing the method for generation of hippocampal-specific *Tob*-KO (hsTobKO) mice through injection of adeno-associated virus expressing Cre recombinase under the hSyn promoter (AAV_hSyn_Cre) in mice having LoxP sequences flanking both sides of the *Tob* gene (*Tob*^{fl/fl}). **F** Contextual fear conditioning and extinction in hsTobKO presented as percentage of time showing freezing. Two-way ANOVA followed by Bonferoni's *post-hoc* test for multiple comparisons. **G** The forced swim test is presented as percentage of time spent immobile. **H** The elevated-plus maze showed as the time spent in the open arm. **I** Open field test showing the percentage of time spent in the center region. Unpaired t-test. All values represent means \pm SEMs. ns non-significant, * $p < 0.05$, ** $p < 0.01$, *** $p < 0.001$, **** $p < 0.0001$.

Similarly, lower levels of p-ERK were observed in the hippocampi of *Tob*-KO mice after the forced swim test, while AAV-mediated *Tob* overexpression in hippocampi of *Tob*-KO mice nullified this effect (Fig. S7A–F). Accordingly, *TOB* deletion repressed stress-induced ERK phosphorylation and simultaneously increased MKP-1 protein levels.

DISCUSSION

Stress vulnerability and resilience differ among individuals, which suggests a strong influence of genetic factors. However, molecular mechanisms predisposing some individuals to stress-induced psychiatric disorders are not well explored. Here, we introduce *TOB* as a psychological stress-responsive gene that governs synchrony between brain regions that process emotional regulation. *Tob*-deficient mice showed abnormal functional dynamics in the hippocampus and between the hippocampus and mPFC. Nonetheless, *Tob* deletion led to impaired hippocampal excitatory-inhibitory balance, accompanied by increased AMPAR- and decreased GABAR-mediated synaptic transmission. Additionally, *TOB*-deficient mice showed abnormal hippocampal-dependent contextual fear conditioning, extinction, and depression-like behaviors. *Tob* deletion resulted in abnormal transient hippocampal transcriptome profiling after fear conditioning in *Tob*-KO mice. Moreover, fear conditioning-induced *Lcn2* expression was suppressed in *Tob*-KO mice, likely through the ERK-mediated pathway (Summarized in Fig. 6).

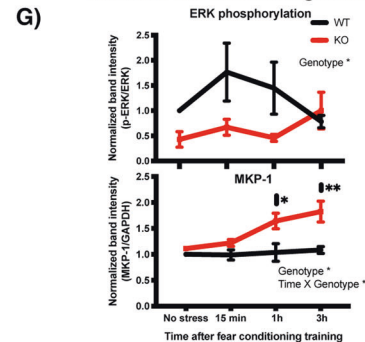
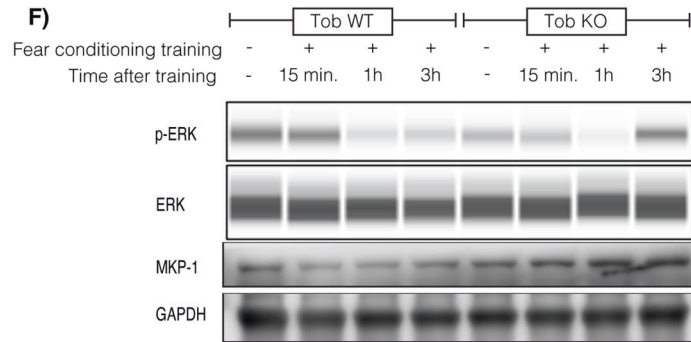
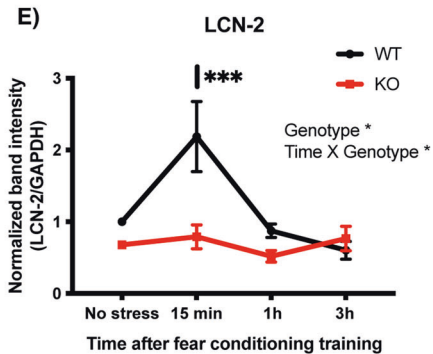
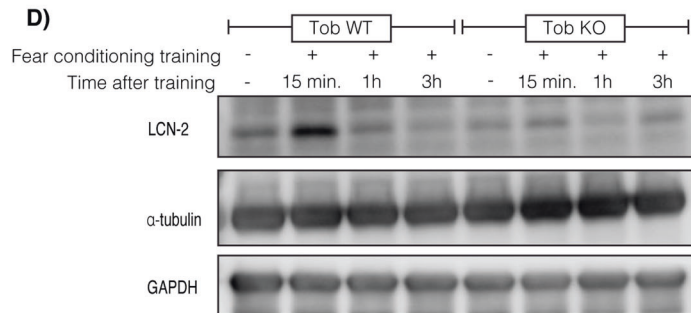
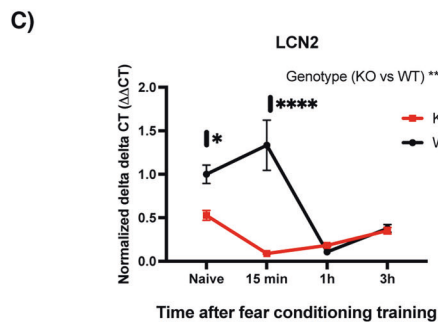
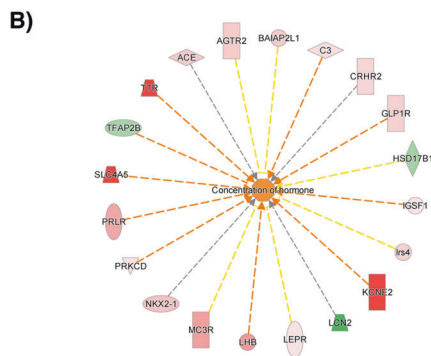
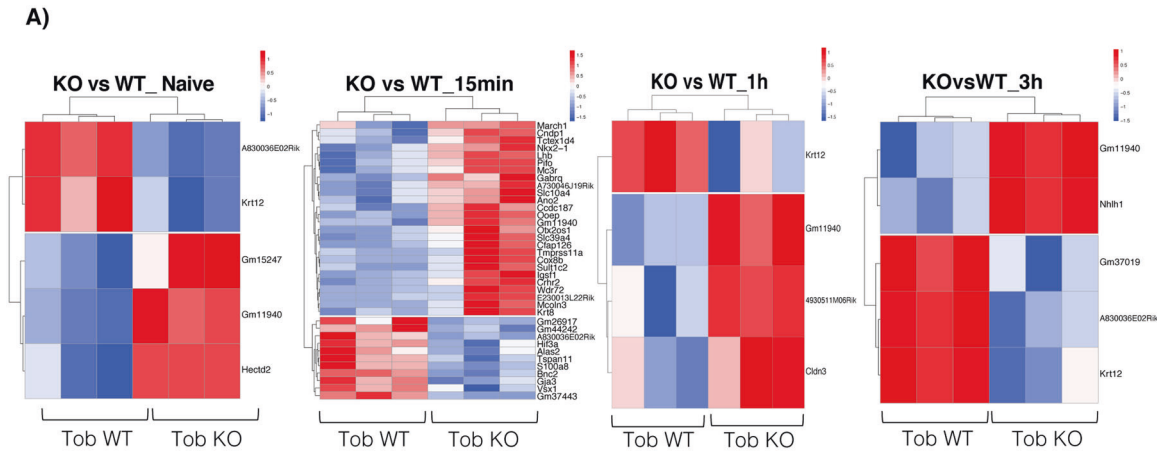
During its initial characterization, *TOB* was proposed to exhibit a transient response to stimulation [49]. Interestingly, *Tob* was recently classified as one of the early response genes [21, 22], possibly due to the presence of three ATTTA motifs in the 3'UTR of the *Tob* gene, which is commonly observed in immediate early genes [50]. Our results show that hippocampal *TOB* levels rapidly increased after acute psychological stress. A similar pattern was observed in genes involved in the stress machinery pathway, like PAI-1 and tPA [51, 52]. Nonetheless, other *TOB* family members, like *Tob2* mRNA in the hippocampus, has been reported to respond to learning cues [53].

Our data show decreased hippocampal-medial-prefrontal functional connectivity in KO mice. Altered PFC connectivity to other brain regions predisposes depression, while enhancement is used to evaluate treatment efficiency [54]. Additionally, the mPFC has an inhibitory function in regulating emotional behavior, like reducing fear responses, extinguishing aversive memories, and suppressing the hypothalamic-pituitary adrenal (HPA) axis [55, 56]. Therefore, decreased functional connectivity in *Tob*-KO mice suggests a loss of inhibitory emotional control of the mPFC over the hippocampus. An aberrant increase of hippocampal CA1-DG functional connectivity in *Tob*-KO mice leads to enhanced synchronization and processing in the hippocampus. Together with the significant increase in the excitatory-inhibitory ratio, our data suggest that hippocampal activity is disproportionately increased. This is consistent with reports of decreased prefrontal

and increased hippocampal activity in PTSD and depression patients [57–60]. One limitation to our fMRI analysis is that the amygdala, a central hub regulating emotional behavior, could not be included due to high noise originating from nearby veins and the air-filled ear canal [61, 62]. There are reports correlating fMRI with neuronal activity [63]. However, it was challenging to distinguish between excitatory and inhibitory neuronal activity in our study. Nonetheless, the change in hippocampal functional connectivity in *Tob*-KO mice suggests a causative change in neuronal activity. The mPFC is anatomically connected to the hippocampus through CA1 [64]. Therefore, we decided to measure CA1 neuronal activity, as we speculated that it helps to regulate hippocampal and mPFC-hippocampal connectivity.

Our results show that *TOB* is expressed in the synaptic fraction, suggesting its possible function in synaptic neurotransmission. This is compatible with a single-cell sequencing study by Qiu et al. [21], which showed a rapid increase in *Tob* expression in excitatory neurons after neuronal stimulation. Our results from *Tob*-deficient hippocampal slices show increased AMPAR-mediated and decreased GABAR-mediated neuronal transmission. Interestingly, increased expression of AMPARs and subsequent neuronal activity were observed in response to stress [65]. On the other hand, decreased inhibitory neurotransmission is a well-established etiology for depression, anxiety, and PTSD [66–68]. Also, inhibiting GABAergic neurons in CA1 altered the hippocampal-mPFC neuronal firing synchronization [69]. As expected, *TOB*-deficient slices show an elevated excitatory/inhibitory (E/I) ratio. A similar increase in E/I ratio is observed in stress and depression mouse models [70–72]. Taken together, the observed change in CA1 neuronal activity of *Tob*-KO mice is strongly linked to the altered functional connectivity between the hippocampus and prefrontal cortex. Additionally, the altered excitation and inhibition balance might be a consequence of decreased inhibitory synaptic transmission [66]. One limitation of our study is that fMRI imaging and electrophysiological recording were done on naive non-stressed mice to analyze basal levels. This was necessary to evaluate abnormal factors leading to altered stress responses. Future measurement of neuronal activity at cellular and circuit levels after stress would offer more insight on the function of *TOB* in the brain's dynamic stress network level.

Fear conditioning and extinction have been introduced as a model of PTSD, to assess emotional behavior in response to aversive stimuli [73]. A stress-induced increase in AMPARs was reported to enhance fear memory [74, 75]. Therefore, elevated hippocampal neurotransmission can be linked to the increased contextual fear conditioning and extinction of *Tob*-KO mice. Our rescue and hippocampal-specific knockout experiments demonstrate that enhanced fear in *Tob*-KO mice is hippocampal-dependent. Forced swim has been implemented to evaluate the ability to cope with inescapable stress [76, 77]. *Tob*-KO mice exhibit depression-like behavior when exposed to forced swim, this suggests that *TOB* may function in efficiently coping with stressors. Such depression-like behavior is consistent with



previously reported low *TOB* mRNA levels in major depressive disorder (MDD) patients [23]. On the other hand, hippocampus-specific *Tob*-KO did not induce anxiety, and *TOB* re-expression in the hippocampus did not reduce it. Therefore, the increased anxiety in *Tob*-KO mice could be mediated by a brain region

other than the hippocampus. This accords with studies showing that anxiety is mainly regulated by the amygdala and prefrontal cortex [78]. Taken together, *TOB* is important for intact hippocampal-mediated stress coping behaviors, namely fear and depression.

Fig. 5 Abnormal transient transcriptional profile in hippocampus of *Tob*-KO mice and suppressed stress-induced LCN2 expression induced after fear conditioning training. **A** Heatmaps for differentially expressed genes in hippocampi of *Tob*-KO compared to *Tob*-WT mice using RNA sequencing without fear conditioning training (naive) and 15 min, 1 h, 3 h after fear conditioning training (represented as z-scores of log raw counts, $FC_{\text{upregulated}} > 2$, $FC_{\text{downregulated}} < 0.5$, $p < 0.05$, $FDR < 0.05$). **B** Pathway analysis for RNA sequencing candidates using IPA software showing activation of hormonal concentration in hippocampus of *Tob* KO mice at 15 min post-conditioning. **C** Real-time PCR for lipocalin-2 (*Lcn2*) mRNA in hippocampus of *Tob*-WT and KO naive mice and 15 min, 1 h and 3 h after fear conditioning. **D** Western blotting showing protein expression of LCN-2 in hippocampi of naive *Tob*-KO mice and at 15 min, 1 h, and 3 h after fear conditioning training. **E** Normalized band intensity for LCN2 protein immunoblots. Two-way ANOVA followed by Bonferoni's *post-hoc* test for multiple comparisons. **F** Western blotting showing abnormal protein expression in hippocampi of mice lacking *Tob* before and after fear conditioning training at 15 min, 1 h and 3 h. **G** Western blot band intensity quantification plots at different time points post-training compared to naive *Tob*-WT (p -ERK $n = 4$, MKP-1 $n = 3$). All values represent means \pm SEMs. ns non-significant, * $p < 0.05$, ** $p < 0.01$, *** $p < 0.001$, **** $p < 0.0001$.

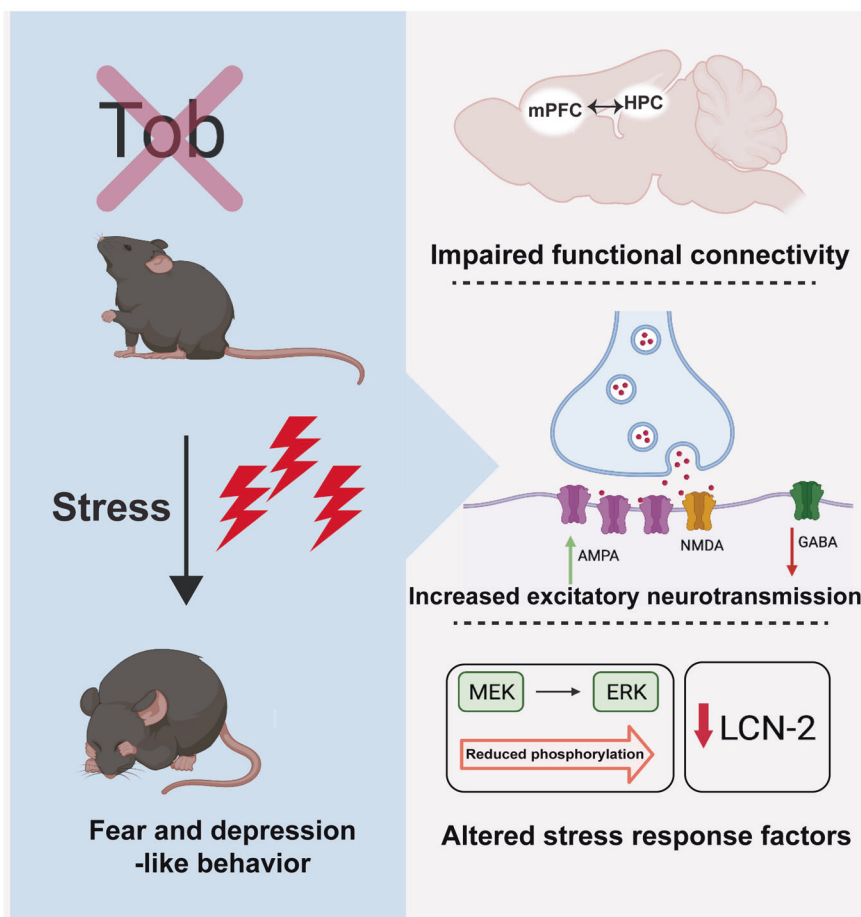


Fig. 6 Summary showing the role of TOB in hippocampus-mediated stress response. *Tob* deletion in mice induces hippocampal-dependent pathological behaviors of increased fear and depression-like behaviors. This can be explained by the altered functional connectivity between stress-related regions like hippocampus (HPC) and medial prefrontal cortex (mPFC). *Tob*-deficient hippocampal neurons showed increased excitatory and decreased inhibitory neurotransmission. Stress-induced ERK phosphorylation and LCN-2 expression were lower in the hippocampus of *Tob*-KO mice.

How does TOB execute stress-induced molecular functions in the hippocampus? TOB regulates gene transcription and mRNA post-transcriptional stability [29, 79, 80]. The transient increase in differentially expressed genes 15 min after fear conditioning in KO mice could be attributed to the functions of TOB in regulating post-transcriptional and post-translational modification processes. These processes can also occur away from the cell body, sometimes locally in the synapse, which might also explain the observed immediate effect. The abnormal changes in hormone receptor levels of KO mice after fear conditioning suggest the activation of stress-induced hormonal pathway. *Ttr*, *Crhr2*, *Avpr1a* and *Mc3r* are among the activated genes that could be involved in this pathway. *Ttr* gene expression is regulated by glucocorticoids

and estradiol [81, 82]. *Crhr2* is activated by Urocotins I, II (stresscopin-related peptide), and III (stresscopin), which belong to the corticotrophin-releasing factor (CRF)-related peptides [83]. *Crhr2* expression in the brain has been correlated with fear [84]. Similarly, elevated *Crhr2* was attributed to an inability to cope with stress, consequently predisposing the individual to PTSD or suicide [85, 86]. Interestingly, stimulating *Crhr2* with different concentrations of agonist, led to either activation or inhibition of the HPA axis [87]. *Avpr1a* is another interesting candidate. Its activation leads to increased fear response and anxiety [88]. Additionally, AVPR1A contributes to activation of the HPA-axis by increasing ACTH and corticosterone levels [89]. Lastly, Melanocortin 3 receptor (*Mc3r*) is another candidate activated by

melanocortin peptides, namely alpha, beta, and gamma-melanocyte-stimulating hormones (MSHs) and adrenocorticotrophic hormone (ACTH)) [90]. MC3R activation has been linked to increased anxiety and stress response [91]. Collectively, the increased mRNA expression of hormone receptor levels in hippocampi of *Tob*-KO mice after fear conditioning may give rise to hormone-mediated abnormal behavior, partly through the hyperactivated HPA axis. This might also be induced by decreased inhibitory neurotransmission, which increases HPA axis activity [92], anxiety, and responses to stress [93].

Fear conditioning induced a transient increase in LCN2 expression in hippocampi of WT mice, which was inhibited by *Tob* deletion. Like *Tob*, *Lcn2* is an acute phase gene [94] that shows increased hippocampal expression in response to restraint stress [95]. Additionally, LCN2 deletion in mice caused anxious- and depressive-like behaviors [96], which resemble those of *Tob*-KO mice. Lower LCN2 expression in TOB-deficient hippocampus can be linked to the observed increase in CA1 excitatory neurotransmission, as LCN2 deficiency induces hippocampal neuronal excitability [95]. Therefore, TOB functions in response to stress may be partially mediated through LCN2. However, until now there has been no evidence showing any interaction between TOB and LCN2. ERK phosphorylation might be the missing link between TOB and LCN2. We observed decreased stress-induced ERK phosphorylation in hippocampus of *Tob*-KO mice. Decreased ERK phosphorylation has been attributed to stress-induced depression [97]. The interaction between TOB and ERK is bidirectional, in that ERK phosphorylates TOB and TOB impacts ERK phosphorylation [26, 98, 99]. On the other hand, ERK phosphorylation induces LCN2 expression [100]. Therefore, it is highly suggestive that decreased LCN2 levels after stress in *Tob*-KO mice are due to altered ERK phosphorylation. The altered stress-induced hippocampal transcription profile after *Tob* deletion, can also be caused by the post-translational changes in ERK. One of the upstream phosphatases controlling ERK phosphorylation is MKP-1, which is overexpressed in hippocampi of *Tob*-KO mice. This is consistent with previous reports that MKP-1 expression is induced by cellular stress and acute glucocorticoid treatment [101], to inactivate MAP kinases such as ERK [102]. The temporal differences between the stress-induced TOB expression and altered molecular pathways, suggest that *Tob* is orchestrating the initiation of the stress coping molecular machinery. Yet, it would be interesting to dissect the functional role of the elevated post-stress TOB in the stress signaling machinery.

In summary, this study demonstrates increased TOB levels after acute stress and highlights its function in the hippocampus by maintaining normal fear and depressive behaviors. We also show that TOB regulates the rapid transcriptional response after acute stress, hippocampal connectivity, and synaptic transmission. These observations set the stage for future use of TOB as a stress biomarker or vulnerability predictor for individuals prone to stress.

REFERENCES

- Kessler RC. The effects of stressful life events on depression. *Annu Rev Psychol.* 1997;48:191–214.
- Cohen S, Janicki-Deverts D, Miller GE. Psychological stress and disease. *JAMA.* 2007;298:1685–7.
- McEwen BS. The neurobiology of stress: from serendipity to clinical relevance. *Brain Res.* 2000;886:172–89.
- Sapolsky RM. Stress and the brain: individual variability and the inverted-U. *Nat Neurosci.* 2015;18:1344–6.
- Chattarji S, Tomar A, Suvrathan A, Ghosh S, Rahman MM. Neighborhood matters: divergent patterns of stress-induced plasticity across the brain. *Nat Neurosci.* 2015;18:1364–75.
- Miyagi T, Oishi N, Kobayashi K, Ueno T, Yoshimura S, Murai T, et al. Psychological resilience is correlated with dynamic changes in functional connectivity within the default mode network during a cognitive task. *Sci Rep.* 2020;10:17760.

- Zhang W, Hashemi MM, Kaldewai R, Koch SBJ, Beckmann C, Klumpers F, et al. Acute stress alters the 'default' brain processing. *Neuroimage.* 2019;189:870–7.
- Battaglia S, Harrison BJ, Fullana MA. Does the human ventromedial prefrontal cortex support fear learning, fear extinction or both? A commentary on sub-regional contributions. *Mol Psychiatry.* 2022;27:784–6.
- Tashjian SM, Zbozinek TD, Mobbs D. A decision architecture for safety computations. *Trends Cogn Sci.* 2021;25:342–54.
- Sinha R, Lacadie CM, Constable RT, Seo D. Dynamic neural activity during stress signals resilient coping. *Proc Natl Acad Sci USA.* 2016;113:8837–42.
- McEwen BS, Nasca C, Gray JD. Stress effects on neuronal structure: hippocampus, amygdala, and prefrontal cortex. *Neuropsychopharmacology.* 2016;41:3–23.
- De Miguel Z, Vegas O, Garmendia L, Arregi A, Beitia G, Azpiroz A. Behavioral coping strategies in response to social stress are associated with distinct neuroendocrine, monoaminergic and immune response profiles in mice. *Behav Brain Res.* 2011;225:554–61.
- Girgenti MJ, Pothula S, Newton SS. Stress and its impact on the transcriptome. *Biol Psychiatry.* 2021;90:102–8.
- Gray JD, Rubin TG, Hunter RG, McEwen BS. Hippocampal gene expression changes underlying stress sensitization and recovery. *Mol Psychiatry.* 2014;19:1171–8.
- Sannino G, Pasqualini L, Ricciardelli E, Montilla P, Soverchia L, Ruggeri B, et al. Acute stress enhances the expression of neuroprotection- and neurogenesis-associated genes in the hippocampus of a mouse restraint model. *Oncotarget.* 2016;7:8455–65.
- Flati T, Gioiosa S, Chillemi G, Mele A, Oliverio A, Mannironi C, et al. A gene expression atlas for different kinds of stress in the mouse brain. *Sci Data.* 2020;7:437.
- Lim CP, Jain N, Cao X. Stress-induced immediate-early gene, *egr-1*, involves activation of p38/JNK1. *Oncogene.* 1998;16:2915–26.
- Duclot F, Kabbaj M. The role of early growth response 1 (EGR1) in brain plasticity and neuropsychiatric disorders. *Front Behav Neurosci.* 2017;11:35.
- Jin M, Wang XM, Tu Y, Zhang XH, Gao X, Guo N, et al. The negative cell cycle regulator, Tob (transducer of ErbB-2), is a multifunctional protein involved in hippocampus-dependent learning and memory. *Neuroscience.* 2005;131:647–59.
- Wang XM, Gao X, Zhang XH, Tu YY, Jin ML, Zhao GP, et al. The negative cell cycle regulator, Tob (transducer of ErbB-2), is involved in motor skill learning. *Biochem Biophys Res Commun.* 2006;340:1023–7.
- Qiu Q, Hu P, Qiu XJ, Govek KW, Camara PG, Wu H. Massively parallel and time-resolved RNA sequencing in single cells with scNT-seq. *Nat Methods.* 2020;17:991.
- Arloth J, Bogdan R, Weber P, Frishman G, Menke A, Wagner KV, et al. Genetic differences in the immediate transcriptome response to stress predict risk-related brain function and psychiatric disorders. *Neuron.* 2015;86:1189–202.
- Kerman IA, Bernard R, Bonney WE, Jones EG, Schatzberg AE, Myers RM, et al. Evidence for transcriptional factor dysregulation in the dorsal raphe nucleus of patients with major depressive disorder. *Front Neurosci-Switz.* 2012;6:135.
- Suzuki T, Tsuzuku J, Kawakami K, Miyasaka T, Yamamoto T. Proteasome-mediated degradation of Tob is pivotal for triggering UV-induced apoptosis. *Oncogene.* 2009;28:401–11.
- Lee HS, Kundu J, Kim RN, Shin YK. Transducer of *erbB-2*. 1 (*tob1*) as a tumor suppressor: a mechanistic perspective. *Int J Mol Sci.* 2015;16:29815–28.
- Che J, Lu YW, Sun KK, Feng C, Dong AJ, Jiao J. Overexpression of TOB1 confers radioprotection to bronchial epithelial cells through the MAPK/ERK pathway. *Oncol Rep.* 2013;30:637–42.
- Usui M, Yoshida Y, Yamashita T, Tsuji K, Ishikawa I, Yamamoto T, et al. Enhancing effect of Tob deficiency on bone formation is specific to bone morphogenetic protein-induced osteogenesis. *J Bone Min Res.* 2002;17:1026–33.
- Saito A, Ochiai K, Kondo S, Tsumagari K, Murakami T, Cavener DR, et al. Endoplasmic reticulum stress response mediated by the PERK-eIF2(α)-ATF4 pathway is involved in osteoblast differentiation induced by BMP2. *J Biol Chem.* 2011;286:4809–18.
- Yoshida Y, Tanaka S, Umemori H, Minowa O, Usui M, Ikematsu N, et al. Negative regulation of BMP/Smad signaling by Tob in osteoblasts. *Cell.* 2000;103:1085–97.
- Shen C, Chen Y-J. Preparation of pre- and post-synaptic density fraction from mouse cortex. *Bio-Protoc.* 2013;3:e880.
- Etherton MR, Tabuchi K, Sharma M, Ko J, Sudhof TC. An autism-associated point mutation in the neuroligin cytoplasmic tail selectively impairs AMPA receptor-mediated synaptic transmission in hippocampus. *EMBO J.* 2011;30:2908–19.
- Ewels PA, Peltzer A, Fillinger S, Patel H, Alneberg J, Wilm A, et al. The nf-core framework for community-curated bioinformatics pipelines. *Nat Biotechnol.* 2020;38:276–8.
- Dobin A, Davis CA, Schlesinger F, Drenkow J, Zaleski C, Jha S, et al. STAR: ultrafast universal RNA-seq aligner. *Bioinformatics.* 2013;29:15–21.

34. Anders S, Pyl PT, Huber W. HTSeq—a Python framework to work with high-throughput sequencing data. *Bioinformatics*. 2015;31:166–9.
35. Robinson MD, McCarthy DJ, Smyth GK. edgeR: a Bioconductor package for differential expression analysis of digital gene expression data. *Bioinformatics*. 2010;26:139–40.
36. Pibiri F, Nelson M, Guidotti A, Costa E, Pinna G. Decreased corticolimbic allo-pregnanolone expression during social isolation enhances contextual fear: a model relevant for posttraumatic stress disorder. *Proc Natl Acad Sci USA*. 2008;105:5567–72.
37. Inoue T, Hoshina N, Nakazawa T, Kiyama Y, Kobayashi S, Abe T, et al. LMTK3 deficiency causes pronounced locomotor hyperactivity and impairs endocytic trafficking. *J Neurosci*. 2014;34:5927–37.
38. Kudo T, Morohashi Y, Yazaki-Sugiyama Y. Early auditory experience modifies neuronal firing properties in the zebra finch auditory cortex. *Front Neural Circuits*. 2020;14:570174.
39. Augustinaite S, Kuhn B. Complementary Ca(2+) activity of sensory activated and suppressed layer 6 corticothalamic neurons reflects behavioral state. *Curr Biol*. 2020;30:3945–3960 e3945.
40. Matsuura K, Mohamed HMA, Youssef MMM, Yamamoto T. Synaptotagmin 2 is ectopically overexpressed in excitatory presynapses of a widely used CaMKIIa-Cre mouse line. *bioRxiv* 2021: 2021.2006.2030.450492.
41. Schulze-Topphoff U, Casazza S, Varrin-Doyer M, Pekarek K, Sobel RA, Hauser SL, et al. Tob1 plays a critical role in the activation of encephalitogenic T cells in CNS autoimmunity. *J Exp Med*. 2013; jem. 20121611.
42. Corvol J-C, Pelletier D, Henry RG, Caillier SJ, Wang J, Pappas D, et al. Abrogation of T cell quiescence characterizes patients at high risk for multiple sclerosis after the initial neurological event. *Proc Natl Acad Sci USA*. 2008;105:11839–44.
43. Rosenberg T, Gal-Ben-Ari S, Dieterich DC, Kreutz MR, Ziv NE, Gundelfinger ED, et al. The roles of protein expression in synaptic plasticity and memory consolidation. *Front Mol Neurosci*. 2014;7:86.
44. Buynitsky T, Mostofsky DL. Restraint stress in biobehavioral research: recent developments. *Neurosci Biobehav Rev*. 2009;33:1089–98.
45. Bali A, Jaggi AS. Electric foot shock stress: a useful tool in neuropsychiatric studies. *Rev Neurosci*. 2015;26:655–77.
46. Kim EJ, Pellman B, Kim JJ. Stress effects on the hippocampus: a critical review. *Learn Mem*. 2015;22:411–6.
47. Myers KM, Davis M. Mechanisms of fear extinction. *Mol Psychiatry*. 2007;12:120–50.
48. Commons KG, Cholanians AB, Babb JA, Ehlinger DG. The rodent forced swim test measures stress-coping strategy, not depression-like behavior. *ACS Chem Neurosci*. 2017;8:955–60.
49. Matsuda S, KawamuraTsuzuku J, Ohsugi M, Yoshida M, Emi M, Nakamura Y, et al. Tob, a novel protein that interacts with p185(erbB2), is associated with anti-proliferative activity. *Oncogene*. 1996;12:705–13.
50. Yoshida Y, Matsuda S, Yamamoto T. Cloning and characterization of the mouse tob gene. *Gene*. 1997;191:109–13.
51. Bouarab C, Roulot-Lacarrière V, Vallée M, Le Roux A, Guette C, Mennesson M, et al. PAI-1 protein is a key molecular effector in the transition from normal to PTSD-like fear memory. *Mol Psychiatry*. 2021;26:4968–81.
52. Pawlak R, Magarinos AM, Melchor J, McEwen B, Strickland S. Tissue plasminogen activator in the amygdala is critical for stress-induced anxiety-like behavior. *Nat Neurosci*. 2003;6:168–74.
53. Poplawski SG, Schoch H, Wimmer M, Hawk JD, Walsh JL, Giese KP, et al. Object-location training elicits an overlapping but temporally distinct transcriptional profile from contextual fear conditioning. *Neurobiol Learn Mem*. 2014;116:90–95.
54. Abdallah CG, Averill LA, Collins KA, Geha P, Schwartz J, Averill C, et al. Ketamine treatment and global brain connectivity in major depression. *Neuropsychopharmacology*. 2017;42:1210–9.
55. Morgan MA, Romanski LM, LeDoux JE. Extinction of emotional learning: contribution of medial prefrontal cortex. *Neurosci Lett*. 1993;163:109–13.
56. Liberzon I, King AP, Britton JC, Phan KL, Abelson JL, Taylor SF. Paralimbic and medial prefrontal cortical involvement in neuroendocrine responses to traumatic stimuli. *Am J Psychiatry*. 2007;164:1250–8.
57. Qin S, Hermans EJ, van Marle HJ, Luo J, Fernandez G. Acute psychological stress reduces working memory-related activity in the dorsolateral prefrontal cortex. *Biol Psychiatry*. 2009;66:25–32.
58. Thomaes K, Dorrepaal E, Draijer NP, de Ruiter MB, Elzinga BM, van Balkom AJ, et al. Increased activation of the left hippocampus region in Complex PTSD during encoding and recognition of emotional words: a pilot study. *Psychiatry Res*. 2009;171:44–53.
59. Werner NS, Meindl T, Engel RR, Rosner R, Riedel M, Reiser M, et al. Hippocampal function during associative learning in patients with posttraumatic stress disorder. *J Psychiatr Res*. 2009;43:309–18.
60. Hao ZY, Zhong Y, Ma ZJ, Xu HZ, Kong JY, Wu Z, et al. Abnormal resting-state functional connectivity of hippocampal subfields in patients with major depressive disorder. *BMC Psychiatry*. 2020;20:71.
61. Boubela RN, Kalcher K, Huf W, Seidel EM, Derntl B, Pezawas L, et al. fMRI measurements of amygdala activation are confounded by stimulus correlated signal fluctuation in nearby veins draining distant brain regions. *Sci Rep*. 2015;5:10499.
62. Li R, Liu X, Sidabras JW, Paulson ES, Jesmanowicz A, Nencka AS, et al. Restoring susceptibility induced MRI signal loss in rat brain at 9.4 T: A step towards whole brain functional connectivity imaging. *PLoS ONE*. 2015;10:e0119450.
63. Heeger DJ, Ress D. What does fMRI tell us about neuronal activity? *Nat Rev Neurosci*. 2002;3:142–51.
64. Jin J, Maren S. Prefrontal-hippocampal interactions in memory and emotion. *Front Syst Neurosci*. 2015;9:170.
65. Whitehead G, Jo J, Hogg EL, Piers T, Kim DH, Seaton G, et al. Acute stress causes rapid synaptic insertion of Ca2+ -permeable AMPA receptors to facilitate long-term potentiation in the hippocampus. *Brain*. 2013;136:3753–65. Pt 12
66. Luscher B, Fuchs T. GABAergic Control of Depression-Related Brain States. Diversity and Functions of GABA Receptors: A Tribute to Hanns Möhler, Part B. 2015: 97–144.
67. Ren Z, Pribiag H, Jefferson SJ, Shorey M, Fuchs T, Stellwagen D, et al. Bidirectional homeostatic regulation of a depression-related brain state by gamma-aminobutyric acid deficits and ketamine treatment. *Biol Psychiatry*. 2016;80:457–68.
68. Kaufman J, Plotsky PM, Nemeroff CB, Charney DS. Effects of early adverse experiences on brain structure and function: clinical implications. *Biol Psychiatry*. 2000;48:778–90.
69. Xia F, Richards BA, Tran MM, Josselyn SA, Takehara-Nishiuchi K, Frankland PW. Parvalbumin-positive interneurons mediate neocortical-hippocampal interactions that are necessary for memory consolidation. *Elife*. 2017;6:e27868.
70. Shi MM, Fan KM, Qiao YN, Xu JH, Qiu LJ, Li X, et al. Hippocampal micro-opioid receptors on GABAergic neurons mediate stress-induced impairment of memory retrieval. *Mol Psychiatry*. 2020;25:977–92.
71. Fee C, Banasr M, Sibille E. Somatostatin-positive gamma-aminobutyric acid interneuron deficits in depression: cortical microcircuit and therapeutic perspectives. *Biol Psychiatry*. 2017;82:549–59.
72. Luscher B, Shen Q, Sahir N. The GABAergic deficit hypothesis of major depressive disorder. *Mol Psychiatry*. 2011;16:383–406.
73. Rau V, DeCola JP, Fanselow MS. Stress-induced enhancement of fear learning: an animal model of posttraumatic stress disorder. *Neurosci Biobehav Rev*. 2005;29:1207–23.
74. Hu H, Real E, Takamiya K, Kang MG, Ledoux J, Huganir RL, et al. Emotion enhances learning via norepinephrine regulation of AMPA-receptor trafficking. *Cell*. 2007;131:160–73.
75. Groc L, Choquet D, Chaouloff F. The stress hormone corticosterone conditions AMPAR surface trafficking and synaptic potentiation. *Nat Neurosci*. 2008;11:868–70.
76. Molendijk ML, de Kloet ER. Coping with the forced swim stressor: current state-of-the-art. *Behav Brain Res*. 2019;364:1–10.
77. de Kloet ER, Molendijk ML. Coping with the forced swim stressor: towards understanding an adaptive mechanism. *Neural Plast*. 2016;2016:6503162.
78. Liu WZ, Zhang WH, Zheng ZH, Zou JX, Liu XX, Huang SH, et al. Identification of a prefrontal cortex-to-amygdala pathway for chronic stress-induced anxiety. *Nat Commun*. 2020;11:2221.
79. Yoshida Y, Nakamura T, Komoda M, Satoh H, Suzuki T, Tsuzuku JK, et al. Mice lacking a transcriptional corepressor Tob are predisposed to cancer. *Genes Dev*. 2003;17:1201–6.
80. Faraji F, Hu Y, Yang HH, Lee MP, Winkler GS, Hafner M, et al. Post-transcriptional control of tumor cell autonomous metastatic potential by CCR4-NOT deadenylase CNOT7. *PLOS Genet*. 2016;12:e1005820.
81. Li X, Masliah E, Reixach N, Buxbaum JN. Neuronal production of transthyretin in human and murine Alzheimer's disease: is it protective? *J Neurosci*. 2011;31:12483–90.
82. Martinho A, Goncalves I, Costa M, Santos CR. Stress and glucocorticoids increase transthyretin expression in rat choroid plexus via mineralocorticoid and glucocorticoid receptors. *J Mol Neurosci*. 2012;48:1–13.
83. Reul JM, Holsboer F. On the role of corticotropin-releasing hormone receptors in anxiety and depression. *Dialogues Clin Neurosci*. 2002;4:31–46.
84. Koorneef LL, Bogaards M, Reinders MJT, Meijer OC, Mahfouz A. How metabolic state may regulate fear: presence of metabolic receptors in the fear circuitry. *Front Neurosci-Switz*. 2018; 12.
85. Hiroi N, Wong ML, Licinio J, Park C, Young M, Gold PW, et al. Expression of corticotropin releasing hormone receptors type I and type II mRNA in suicide victims and controls. *Mol Psychiatry*. 2001;6:540–6.
86. Toth M, Flandreau EI, Deslauriers J, Geyer MA, Mansuy IM, Merlo Pich E, et al. Overexpression of forebrain CRH during early life increases trauma susceptibility in adulthood. *Neuropsychopharmacology*. 2016;41:1681–90.
87. Bagosi Z, Csabafi K, Palotai M, Jaszberenyi M, Foldesi I, Gardi J, et al. The interaction of Urocortin II and Urocortin III with amygdalar and hypothalamic

- corticotropin-releasing factor (CRF)—reflections on the regulation of the hypothalamic-pituitary-adrenal (HPA) axis. *Neuropeptides*. 2013;47:333–8.
88. Carter CS. The oxytocin-vasopressin pathway in the context of love and fear. *Front Endocrinol (Lausanne)*. 2017;8:356.
 89. Zhu J, Chen Z, Zhu L, Meng Z, Wu G, Tian Z. Arginine vasopressin and arginine vasopressin receptor 1b involved in electroacupuncture-attenuated hypothalamic-pituitary-adrenal axis hyperactivity in hepatectomy rats. *Neuro-modulation*. 2016;19:498–506.
 90. Bertolini A, Tacchi R, Vergoni A. Brain effects of melanocortins. *Pharmacol Res*. 2009;59:13–47.
 91. Gogas KR, Lechner SM, Markison S, Williams JP, McCarthy W, Grigoriadis DE, et al. 6.04 - Anxiety. In: Taylor JB, Triggler DJ (eds). *Comprehensive Med Chem. II*. Elsevier: Oxford, 2007, pp 85–115.
 92. Shen Q, Lal R, Luellen BA, Earnheart JC, Andrews AM, Luscher B. gamma-Aminobutyric acid-type A receptor deficits cause hypothalamic-pituitary-adrenal axis hyperactivity and antidepressant drug sensitivity reminiscent of melancholic forms of depression. *Biol Psychiatry*. 2010;68:512–20.
 93. Crestani F, Lorez M, Baer K, Essrich C, Benke D, Laurent JP, et al. Decreased GABAA-receptor clustering results in enhanced anxiety and a bias for threat cues. *Nat Neurosci*. 1999;2:833–9.
 94. Liu Q, Nilsen-Hamilton M. Identification of a new acute phase protein. *J Biol Chem*. 1995;270:22565–70.
 95. Mucha M, Skrzypiec AE, Schiavon E, Attwood BK, Kucerova E, Pawlak R. Lipocalin-2 controls neuronal excitability and anxiety by regulating dendritic spine formation and maturation. *Proc Natl Acad Sci USA*. 2011;108:18436–41.
 96. Ferreira AC, Pinto V, Da Mesquita S, Novais A, Sousa JC, Correia-Neves M, et al. Lipocalin-2 is involved in emotional behaviors and cognitive function. *Front Cell Neurosci*. 2013;7:122.
 97. Dwivedi Y, Zhang H. Altered ERK1/2 signaling in the brain of learned helpless rats: relevance in vulnerability to developing stress-induced depression. *Neural Plast*. 2016;2016:7383724.
 98. Maekawa M, Nishida E, Tanoue T. Identification of the anti-proliferative protein Tob as a MAPK substrate. *J Biol Chem*. 2002;277:37783–7.
 99. Suzuki T, K-Tsuzuku J, Ajima R, Nakamura T, Yoshida Y, Yamamoto T. Phosphorylation of three regulatory serines of Tob by Erk1 and Erk2 is required for Ras-mediated cell proliferation and transformation. *Genes Dev*. 2002;16:1356–70.
 100. Du ZP, Wu BL, Xie YM, Zhang YL, Liao LD, Zhou F, et al. Lipocalin 2 promotes the migration and invasion of esophageal squamous cell carcinoma cells through a novel positive feedback loop. *Biochim Biophys Acta*. 2015;1853:2240–50.
 101. Maitra U, Deng H, Glaros T, Baker B, Capelluto DG, Li Z, et al. Molecular mechanisms responsible for the selective and low-grade induction of proinflammatory mediators in murine macrophages by lipopolysaccharide. *J Immunol*. 2012;189:1014–23.
 102. Clark AR, Lasa M. Crosstalk between glucocorticoids and mitogen-activated protein kinase signalling pathways. *Curr Opin Pharm*. 2003;3:404–11.

ACKNOWLEDGEMENTS

This work was financially supported by Okinawa Institute of Science and Technology Graduate University and JSPS Fellowship and Kakenhi grants number 18J20551. We thank Prof. Yoko Yazaki-Sugiyama and Dr. Yuichi Morohashi for their support in generating Tob AAV viral vectors. pAAV-hSyn-EGFP was a gift from Bryan Roth

(Addgene plasmid # 50465), pAdDeltaF6, pAAV2/9n, pENN.AAV.hSyn.Cre.WPRE.hGH were gifts from James M. Wilson (Addgene plasmid # 112867, 112865, Addgene viral prep # 105553-AAV1). Illustrative figures were created with Biorender.com. We are grateful for the help and support provided by the animal resources, high-performance computing, and sequencing sections of the Research Support Division at Okinawa Institute of Science and Technology Graduate University.

AUTHOR CONTRIBUTIONS

MY and TY conceived the idea and coordinated the study. MY performed the behavioral experiments, molecular experiments, and bioinformatic analyses. HH performed fMRI. EL performed electrophysiological recording. ME and BK performed stereotaxic surgery and viral injections. YK performed elevated-plus maze and provided support for behavioral analysis. HK and KN generated Tob^{fl/+} mice. MY, EL, HH, ME, and TY participated in manuscript writing. All authors revised and approved the final version of manuscript.

COMPETING INTERESTS

The authors declare no competing interests.

ADDITIONAL INFORMATION

Supplementary information The online version contains supplementary material available at <https://doi.org/10.1038/s41398-022-02078-7>.

Correspondence and requests for materials should be addressed to Mohieldin M. M. Youssef or Tadashi Yamamoto.

Reprints and permission information is available at <http://www.nature.com/reprints>

Publisher's note Springer Nature remains neutral with regard to jurisdictional claims in published maps and institutional affiliations.



Open Access This article is licensed under a Creative Commons Attribution 4.0 International License, which permits use, sharing, adaptation, distribution and reproduction in any medium or format, as long as you give appropriate credit to the original author(s) and the source, provide a link to the Creative Commons license, and indicate if changes were made. The images or other third party material in this article are included in the article's Creative Commons license, unless indicated otherwise in a credit line to the material. If material is not included in the article's Creative Commons license and your intended use is not permitted by statutory regulation or exceeds the permitted use, you will need to obtain permission directly from the copyright holder. To view a copy of this license, visit <http://creativecommons.org/licenses/by/4.0/>.

© The Author(s) 2022